Citrullinated human and murine MOG35-55 display distinct biophysical and biochemical behavior

Doelman, W.; Reijnen, R.C.; Dijksman, N.; Janssen, A.P.A.; Driel, N. van; Hart, B.A.; ... ; Kasteren, S.I. van

Citrullinated human and murine $MOG_{35–55}$ display distinct biophysical and biochemical behavior

Received for publication, January 8, 2023, and in revised form, February 15, 2023 Published, Papers in Press, February 24, 2023,
https://doi.org/10.1016/j.jbc.2023.103065

W. Doelman[1], R. C. Reijnen[1], N. Dijksman[2], A. P. A. Janssen[1], N. van Driel[3], B. A. 't Hart[2], I. Philippens[3], C. Araman[1], W. Baron[2,*], and S. I. van Kasteren[1,*]

From the [1]Department of Bio-Organic Synthesis, Leiden Institute of Chemistry, Leiden, the Netherlands; [2]Section Molecular Neurobiology, Department Biomedical Sciences of Cells & Systems, University Medical Center Groningen, University of Groningen, Groningen, the Netherlands; [3]Department of Immunobiology, Biomedical Primate Research Center, Rijswijk, the Netherlands

Reviewed by members of the JBC Editorial Board. Edited by Joan B. Broderick

The peptide spanning residues 35 to 55 of the protein myelin oligodendrocyte glycoprotein (MOG) has been studied extensively in its role as a key autoantigen in the neuroinflammatory autoimmune disease multiple sclerosis. Rodents and nonhuman primate species immunized with this peptide develop a neuroinflammatory condition called experimental autoimmune encephalomyelitis, often used as a model for multiple sclerosis. Over the last decade, the role of citrullination of this antigen in the disease onset and progression has come under increased scrutiny. We recently reported on the ability of these citrullinated MOG35–55 peptides to aggregate in an amyloid-like fashion, suggesting a new potential pathogenic mechanism underlying this disease. The immunodominant region of MOG is highly conserved between species, with the only difference between the murine and human protein, a polymorphism on position 42, which is serine in mice and proline for humans. Here, we show that the biophysical and biochemical behavior we previously observed for citrullinated murine MOG35–55 is fundamentally different for human and mouse MOG35–55. The citrullinated human peptides do not show amyloid-like behavior under the conditions where the murine peptides do. Moreover, we tested the ability of these peptides to stimulate lymphocytes derived from MOG immunized marmoset monkeys. While the citrullinated murine peptides did not produce a proliferative response, one of the citrullinated human peptides did. We postulate that this unexpected difference is caused by disparate antigen processing. Taken together, our results suggest that further study on the role of citrullination in MOG-induced experimental autoimmune encephalomyelitis is necessary.

Multiple sclerosis (MS) is a family of autoimmune-driven neurological diseases that present themselves pathologically in the form of neuroinflammation, demyelination, and axonal damage (1). Most patients (∼85%) start with the relapsing-remitting form of the disease, where episodes of neurological impairment (relapse) alternate with symptom-free periods (remission). A large proportion (∼60%) of these patients later progresses into secondary progressive MS, where neurological damage is chronic, and remissions no longer occur. A small but not negligible portion of the patients (10–15%) starts off with a progressive form of the disease, called primary progressive MS (2). While treatments exist to manage the relapsing form of the disease, the progressive forms are debilitating and currently untreatable (3). Risk factors for the development of MS include genetic factors (4), low vitamin D levels (5) and infection with Epstein–Barr virus (EBV) (6, 7).

Currently, the precise molecular mechanisms underlaying the development of the different forms of MS and their relation to these risk factors are unknown (8). Most research on the mechanisms of disease onset and progression is carried out using rodent and nonhuman primate models. One such disease model used for MS mechanistic studies is experimental autoimmune encephalomyelitis (EAE) (9). Here, induction of the disease is usually accomplished by immunization with myelin antigens, for instance myelin basic protein (10), proteolipid protein (11), or myelin oligodendrocyte glycoprotein (MOG), typically in combination with a strong immune adjuvant, such as complete Freund's adjuvant (CFA).

MOG is a membrane-bound glycoprotein (∼26 kDa) highly conserved between mammalian species. The protein has an extracellular domain with an immunoglobulin-like fold containing a single *N*-glycosylation site at position 31 (12, 13). When inducing EAE with MOG, either a nonglycosylated recombinant protein covering the extracellular part of the protein, $MOG_{1–125}$ (14), or a peptide covering an immunodominant region, $MOG_{35–55}$ (15), is used, usually in combination with CFA, which contains heat-inactivated mycobacterial components suspended in mineral oil to induce an immune response. The immunodominant peptide $MOG_{35–55}$ is part of a highly conserved region of the MOG protein (residues 20–50) (Fig. 1*A*), with a single amino acid polymorphism on position 42, the only difference between common animal models. Mouse, rat, and the common marmoset (*Callithrix jacchus*) share a serine at position 42 (from here on referred to as mMOG). Higher primates (including human and rhesus monkey), as well as most other species (see Table S1 for an overview), have a proline at this

* For correspondence: S. I. van Kasteren, s.i.van.kasteren@chem.leidenuniv.nl; W. Baron, w.baron@umcg.nl.

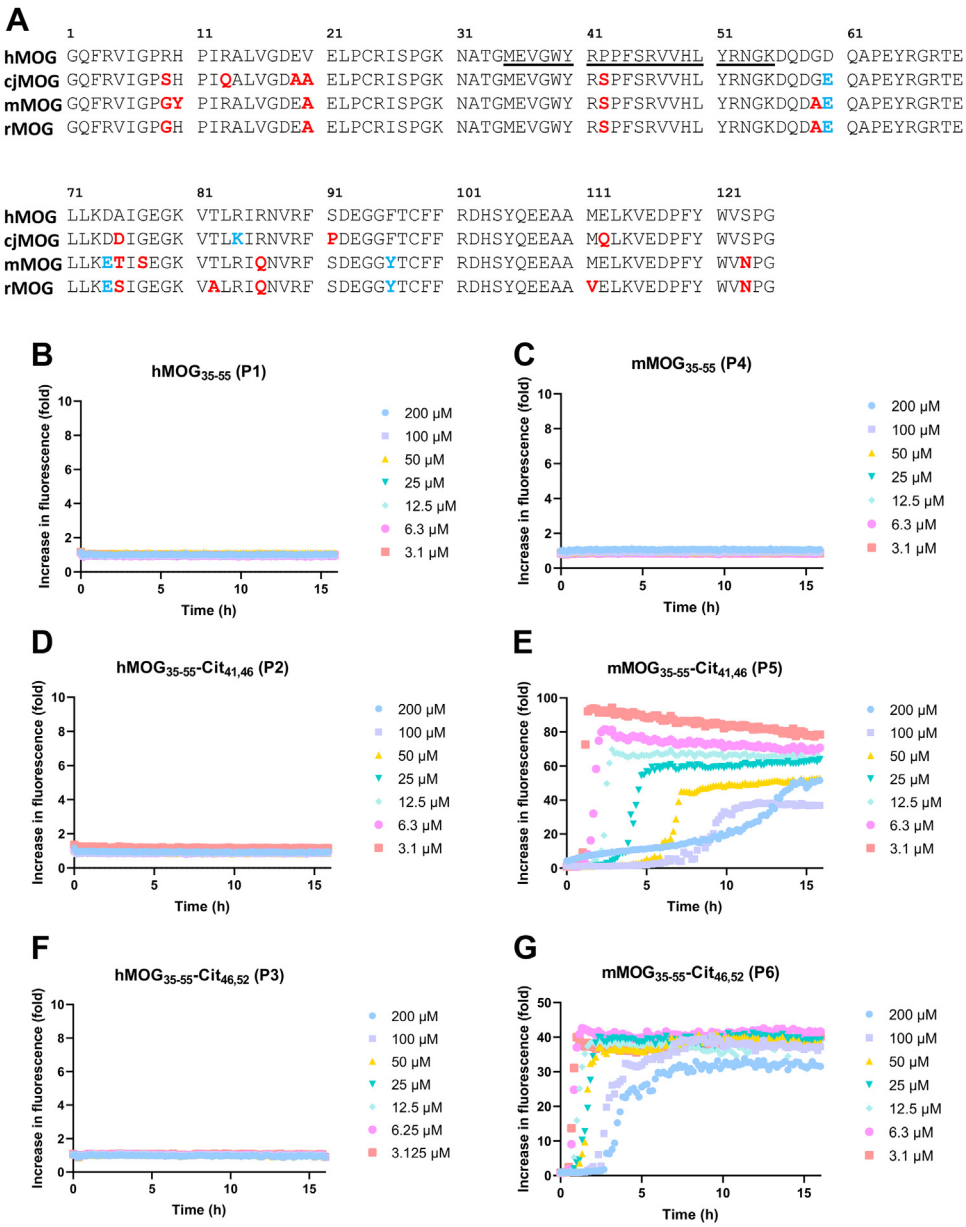

Figure 1. Comparison of the MOG$_{35-55}$ sequence of different species and the effect of the amino acid polymorphism on the citrullination-induced amyloid-like aggregation. *A,* amino acid sequence of the extracellular part of myelin oligodendrocyte glycoprotein (MOG) for human (hMOG), common marmoset (*Callithrix jacchus*) (cjMOG), mouse (mMOG), and rat (rMOG). Residues that are mutated compared with the human protein are marked *red*, whereas minor mutations are marked in *blue*. The immunodominant portion, MOG$_{35–55}$, is *underlined*. *B–G*, thioflavin T (ThT) aggregation assays showing the aggregation properties of hMOG$_{35–55}$ (P1–3) and mMOG$_{35–55}$ (P4–6) and their citrullinated variants at pH 5.0 (20 mM NaOAc buffer) and 37 °C.

position (from here referred to as hMOG). As part of our ongoing research into the role of MOG in EAE and MS initiation and progression, we set out to better characterize the biological effect of this single amino acid polymorphism.

In a previous work in a translationally relevant MS animal model, EAE in the common marmoset (*C. jacchus*) revealed contrasting results between immunization with the peptide and protein. Immunization with hMOG$_{34–56}$ in incomplete Freund's adjuvant (IFA; a mineral oil lacking the mycobacteria component of CFA) was able to induce EAE, indicating some level of immunostimulatory ability of the peptide itself. In contrast, when recombinant hMOG$_{1–125}$ protein in IFA was used to induce EAE, no immune response against the otherwise immunodominant peptide MOG$_{34–56}$ was observed (16). We hypothesized this to be the result of altered proteolysis of MOG, resulting from citrullination of the protein.

Citrullination is the biochemical transformation of positively charged arginine into neutral citrulline, catalyzed by a family of enzymes called the peptide arginyl deamidases (17). Increased citrullination of myelin proteins has been observed as a molecular hallmark of MS, with several proteins affected (18–20). Earlier work in a rodent MS model also highlighted the effects of this post-translational modification on the immunogenic properties of myelin antigens (21). We previously hypothesized that the citrullination of MOG antigens

could take place inside EBV-infected B cells, which are known to overexpress peptide arginyl deamidases (22). Involvement of B cells in disease progression has been shown in patients, where B-cell depletion by ocrelizumab, an antibody targeting the B-cell marker CD20, has positive clinical outcomes (23). Furthermore, we showed that citrullination of $MOG_{35–55}$ peptides on the Arg_{46} position inhibits their degradation, both *in vitro* and in EBV-infected B cells (22, 24).

Recently, we studied the effects of citrullination of $mMOG_{35–55}$ on the biophysical properties of the peptide and found that citrullination induced amyloid-like aggregation of this peptide (25). Amyloid-like aggregation is the formation of a stable and usually cross–beta-sheet secondary structure of a protein or a peptide, which is able to induce the further aggregation of free peptide or protein (26). Two dicitrullinated variants, $mMOG_{35–55}$-$Cit_{41,46}$ and $mMOG_{35–55}$-$Cit_{46,52}$ were further found—in contrast to the noncitrullinated control—to not be recognized by T lymphocytes of $hMOG_{35–55}$-immunized marmosets. Instead, they showed cytotoxicity to the antigen-presenting B cells and T cells in coculture.

As stated earlier, $mMOG_{35–55}$ and $hMOG_{35–55}$ differ by a single amino acid, with hMOG carrying a proline at position 42 and mMOG a serine. We were curious whether this Pro-to-Ser polymorphism influences the citrulline-dependent amyloid-like aggregation, as single amino-acid mutations of the $A\beta_{40}$ peptide, the amyloidogenic peptide involved in Alzheimer's disease, have been shown to both aggravate (27) or decrease (28) the ability of this peptide to form amyloid fibrils. In addition, a single amino acid substitution in the flexible tail region of prion protein has recently also been shown to abolished prion toxicity (29). We were also interested in the effect of this mutation on the recognition of the citrulline-modified peptide by T cell in a B-cell crosspresentation assay, as we and others (21) have previously shown that citrullination of $mMOG_{35–55}$ can abolish this peptide's immunogenicity. Here, we report our first results showing that human and murine $MOG_{35–55}$ present fundamentally different behavior *in vitro* after post-translational citrullination. We found that the pronounced amyloid-like aggregation we previously reported for citrullinated $mMOG_{35–55}$ is completely absent when the citrullinated human peptides are evaluated under the same conditions. Furthermore, unlike the murine citrullinated peptides that were previously shown to not be antigenic in the marmoset model, one of the human citrullinated peptides was able to induce T-cell proliferation at a physiologically relevant concentration.

Results

Ser_{42} is critical for citrulline-dependent $MOG_{35–55}$ aggregation

Initially, we set out to determine the effect of the human serine-to-proline mutation on the citrulline-dependent amyloid-like aggregation of our previously established panel of citrullinated $mMOG_{35–55}$ peptides (25). $hMOG_{35–55}$ peptides containing the same modifications, that is dicitrullination on either $Arg_{41,46}$ or $Arg_{46,52}$, as well as the noncitrullinated variants, were synthesized. For the synthesis, TentaGel S RAM resin was used, resulting in C-terminally amidated peptides (Table 1, P1–6). Their aggregation properties compared with $mMOG_{35–55}$ were established using the previously described conditions. This assay involves incubating the peptide under investigation at different concentrations at pH 5.0 and 37 °C in the presence of the fluorogenic dye thioflavin T (ThT) for up to 16 h (30). This dye shows a large shift in fluorescence emission once bound to the typical cross–beta strands of amyloids, thereby enabling the monitoring of the formation of amyloid-like aggregates. In this assay, neither the wildtype human (P1, Fig. 1*B*) nor the mouse $MOG_{35–55}$ (P4, Fig. 1*C*) showed an increase of ThT fluorescence over time, confirming that noncitrullinated $MOG_{35–55}$ does not aggregate under these conditions. As expected, the murine $mMOG_{35–55}$-$Cit_{41,46}$ (P5, Fig. 1*E*) and $mMOG_{35–55}$-$Cit_{46,52}$ (P6, Fig. 1*G*) showed a strong increase in ThT fluorescence over time. Unexpectedly however, the human variants $hMOG_{35–55}$-$Cit_{41,46}$ (P2, Fig. 1*D*) and $hMOG_{35–55}$-$Cit_{46,52}$ (P3, Fig. 1*F*) did not show any increase in ThT fluorescence over the course of the experiment.

Table 1
Overview of synthetic citrullinated $MOG_{35–55}$ derivatives

Code	Name	Sequence[a]	t_{50} at 12.5 μM (h)[b]
P1	$hMOG_{35–55}$	MEVGWYRPPFSRVVHLYRNGK	—
P2	$hMOG_{35–55}$-$Cit_{41,46}$	MEVGWY*Cit*PPFCitVVHLYRNGK	—
P3	$hMOG_{35–55}$-$Cit_{46,52}$	MEVGWYRPPFS*Cit*VVHLY*Cit*NGK	—
P4	$mMOG_{35–55}$	MEVGWYR**S**PFSRVVHLYRNGK	—
P5	$mMOG_{35–55}$-$Cit_{41,46}$	MEVGWY*Cit***S**PF*Cit*VVHLYRNGK	2.4 ± 0.02
P6	$mMOG_{35–55}$-$Cit_{46,52}$	MEVGWYR**S**PFS*Cit*VVHLY*Cit*NGK	1.1 ± 0.03
P7	$MOG_{35–55}$-Ala_{42}-$Cit_{41,46}$	MEVGWY*Cit***A**PF*Cit*VVHLYRNGK	—
P8	$MOG_{35–55}$-Ala_{42}-$Cit_{46,52}$	MEVGWYR**A**PFS*Cit*VVHLY*Cit*NGK	7.3 ± 0.16
P9	$MOG_{35–55}$-Thr_{42}-$Cit_{41,46}$	MEVGWY*Cit*TPF*Cit*VVHLYRNGK	—
P10	$MOG_{35–55}$-Thr_{42}-$Cit_{46,52}$	MEVGWYR**T**PFS*Cit*VVHLY*Cit*NGK	—
P11	$MOG_{35–55}$-Abu_{42}-$Cit_{41,46}$	MEVGWY*Cit****Abu***PF*Cit*VVHLYRNGK	5.2 ± 0.05
P12	$MOG_{35–55}$-Abu_{42}-$Cit_{46,52}$	MEVGWYR***Abu***PFS*Cit*VVHLY*Cit*NGK	—
P13	$MOG_{35–55}$-Hyp_{42}-$Cit_{41,46}$	MEVGWY*Cit****Hyp***PF*Cit*VVHLYRNGK	—
P14	$MOG_{35–55}$-Hyp_{42}-$Cit_{46,52}$	MEVGWYR***Hyp***PFS*Cit*VVHLY*Cit*NGK	—
P15	$hMOG_{35–55}$-Hyp_{43}-$Cit_{41,46}$	MEVGWY*Cit*P***Hyp***F*Cit*VVHLYRNGK	—
P16	$hMOG_{35–55}$-Hyp_{43}-$Cit_{46,52}$	MEVGWYRP***Hyp***FS*Cit*VVHLY*Cit*NGK	—

Amino acids are indicated with the canonical one-letter code.
Abbreviations: Cit, citrulline; Hyp, 4-hydroxyproline.
[a] The amino acid that differs from the sequence of $hMOG_{35–55}$ is highlighted in boldface.
[b] t_{50} is the time for the ThT signal to reach 50% of the plateau (31). — indicates no aggregation was observed. Numbers are given with 95% confidence interval.

We also attempted to induce aggregation of the citrullinated hMOG peptides by coincubation with seeds formed from $mMOG_{35–55}$-$Cit_{46,52}$ as described previously (25), but no aggregation was observed (Fig. S1).

We next studied whether this inhibition of aggregation was specifically caused by substitution of serine by proline on position 42, as this is the only difference between these peptides (Fig. 1*A*). To better understand the importance of this serine residue, we synthesized a series of peptides carrying different amino acid substitutions at position 42, bearing either the $Cit_{41,46}$ or $Cit_{46,52}$ citrullination pattern, and assessed whether these aggregated (Table 1, P7–16). We envisioned that, if proline was indeed inhibitory, then structurally close analogs of serine, like alanine and threonine or the unnatural serine isostere L-2-aminobutyric acid (Abu), should show comparable aggregation behavior. The alanine mutants of both dicitrullinated forms are shown in Figure 2, *A* and *B*. P8 showed clear increase of ThT fluorescence at the lower concentrations, although onset of aggregation was slowed compared with the serine peptide. We fitted the aggregation data according to Equation 1 and used these fits to determine the change in t_{lag} (defined as the time point at which the ThT fluorescence reaches 10% of the maximum value) and t_{50} (time point at which 50% of maximum ThT fluorescence is reached) (31). By this method, we found that, at a concentration of 12.5 μM, Δt_{lag} = 3.7 h and Δt_{50} = 6.3 h (compared with P6). The version bearing citrulline at positions 41 and 46 (P7), on the other hand, showed very little increase in ThT fluorescence even after 16 h. For the threonine mutant, no increase in ThT fluorescence was observed for both P9 and P10 (Fig. 2, *C* and *D*). The peptides containing Abu, an unnatural isostere of serine that should be a closer aliphatic structural mimic of serine than alanine, also showed erratic aggregation behavior. P11 showed fast aggregating behavior at the lower concentrations (Fig. 2*E*), although not in a very consistent manner, as repeated assays produced very different curves, as shown in Fig. S2. We again fitted the data according to Equation 1 and compared this with $mMOG_{35–55}$-$Cit_{41,46}$ (P5) and found Δt_{lag} = 2.3 h and Δt_{50} = 2.7 h (at a concentration of 12.5 μM). The Abu containing peptide with citrulline on positions 46 and 52 (P12) did not show any increase in ThT fluorescence after 16 h (Fig. 2*F*).

We next assessed whether the hydroxylation of Pro_{42} would increase the human peptide's propensity to aggregate. Proline hydroxylation is a post-translational modification not only important for collagen stability but also relevant to other biochemical mechanisms such as oxygen sensing (32). Citrullinated $hMOG_{35–55}$ peptides containing 4-hydroxyproline in place of Pro_{42} were synthesized (P13 and P14), and their aggregation behavior was evaluated. No increase in ThT fluorescence was observed for these peptides after 16 h (Fig. 2, *G* and *H*). Hydroxylation of the other proline residues in the core of $MOG_{35–55}$, Pro_{43}, was also evaluated. Two peptides bearing this modification (P15 and P16) were also synthesized, but no increase in ThT fluorescence was observed again (Fig. S3).

To validate the results obtained from the ThT assays, we also investigated the aggregation of hMOG and mMOG peptides when fed to EBV-infected B cells. To visualize the aggregates, the fluorogenic dye, thioflavin S (ThS), a chemically modified form of ThT that is more suitable for microscopy studies, was employed (33). In the absence of peptide, no aggregates were stained with ThS (Fig. 3*A*). hMOG-peptides P1, P2, and P3 did not show positive ThS staining (Fig. 3, *B–D*), supporting the results of the ThT assays (Fig. 1, *B*, *D* and *F*). Peptide P6 ($mMOG_{35–55}$-$Cit_{46,52}$) exhibited punctate ThS staining under standard culture conditions, although only in very low numbers (Fig. 3*G*, *arrow*). However, for murine peptides P4 and P5, no detectable aggregates were observed (Fig. 3, *E* and *F*).

$hMOG_{35–55}$-$Cit_{46,52}$, but not $mMOG_{35–55}$-$Cit_{46,52}$, shows T-cell activation in a marmoset B-cell crosspresentation assay

We have previously compared the immunogenicity of peptides P4, P5, and P6 in a marmoset B-cell crosspresentation assay. Here, we found that both citrullinated peptides—in contrast to the unmodified peptide—failed to elicit T-cell proliferation. To understand whether this also holds true for the human MOG-derived sequences, we performed this T-cell activation assay on P1–6. To this end, we used cells isolated from the axillary lymph node (ALN) of marmosets immunized using the previously described $hMOG_{1–125}$/IFA protocol as responder cells (16) and carried out the crosspresentation assay as described (25). Briefly, EBV-infected marmoset B-lymphoblastoid cells were lethally irradiated at 70 Gy and incubated with different concentrations (10, 3, and 1 μM) of the peptides for 1 h. After this incubation period, freshly thawed marmoset ALN cells were added to the B-lymphoblastoid cell culture and cocultured for 48 h, and the proliferation of the lymphocyte cells was determined *via* a [^{3}H] thymidine incorporation assay. From this assay, a stimulation index (ratio of proliferation of treated cells *versus* untreated control) was calculated, and a stimulation index >2 was considered T-cell activation. The results of this assay are plotted in Figure 4.

Both wildtype peptides $hMOG_{35–55}$ (P1) and $mMOG_{35–55}$ (P4) induced a proliferative response at the highest concentration of 10 μM. $hMOG_{35–55}$ also showed proliferation at lower concentrations. When both Arg_{41} and Arg_{46} are citrullinated (P2 and P5), no T-cell response was measured for both the human and murine peptides, as reported previously in mouse models (21). The (nonaggregating) $hMOG_{35–55}$-$Cit_{46,52}$ (P3), however, did show T-cell proliferation for two of the three tested animals. Its aggregating murine counterpart P6 in contrast did not.

Truncated version of $mMOG_{35–55}$-$Cit_{46,52}$ display severely reduced aggregation

As crosspresentation of an antigenic peptide to T cells involves the degradation of the longer peptide into the major histocompatibility complex class I-binding epitope, we were interested whether shorter peptides derived from murine MOG would have amyloidogenic properties of their own. In the marmoset system, the nonapeptide $MOG_{40–48}$ had

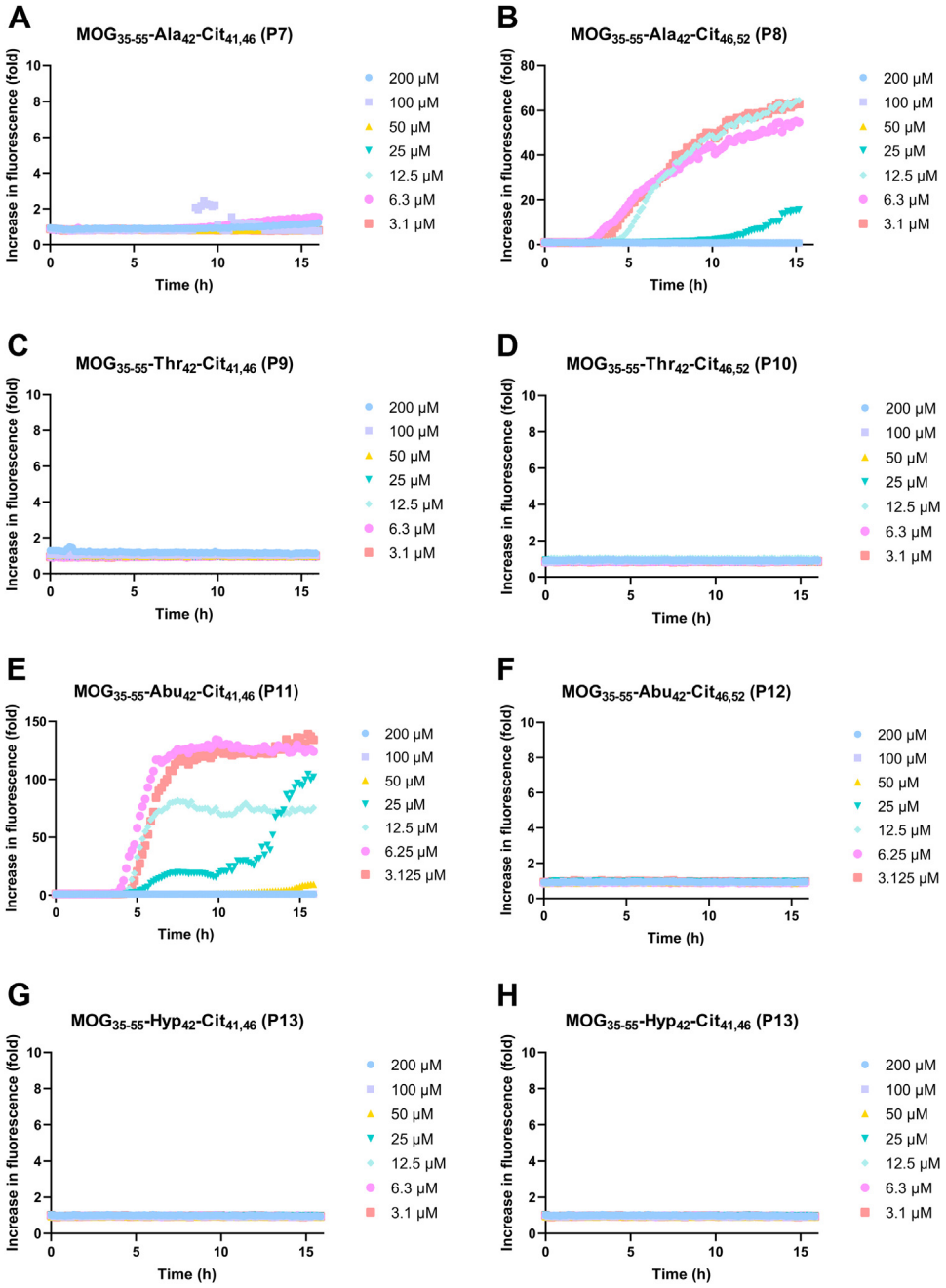

Figure 2. Thioflavin T (ThT) aggregation assays showing the aggregation properties of MOG$_{35–55}$-Cit$_{41,46}$ and MOG$_{35–55}$-Cit$_{46,52}$. When Ser$_{42}$ is replaced with either alanine (*A* and *B*), threonine (*C* and *D*), L-2-aminobutyric acid (Abu) (*E* and *F*), or L-4-hydroxyproline (Hyp) (*G* and *H*). MOG, myelin oligodendrocyte glycoprotein.

previously been identified as the immunodominant T-cell epitope (34). This peptide contains two of the three arginine residues that induce aggregation upon citrullination. We synthesized the three possible citrullinated permutations of this peptide (P17–19, Table 2) and subjected them to evaluation in the ThT assay (Figs. 5*A* and S4). We found that these peptides showed no increase in ThT fluorescence at any concentration tested.

To establish the minimal aggregating sequence of citrullinated murine MOG, a series of stepwise N- and C-terminally extended peptides was synthesized, all containing citrulline at position 46 (P20–25, Table 2). The aggregation properties of these were determined in a full concentration range (Fig. S4). To summarize the data, Figure 5*B* shows a comparison of all peptides at 50 µM, with full concentration ranges given in Fig. S5. The shortest peptide that showed a positive signal in the ThT assay was P23 (mMOG$_{36–52}$-Cit$_{46}$). When the peptide was extended further by one amino acid on both termini to give mMOG$_{35-–53}$-Cit$_{46,52}$ (P25), an aggregation profile similar to mMOG$_{35–55}$-Cit$_{46,52}$ was obtained (Fig. 1*G*). We also synthesized the 46,52 dicitrullinated form of mMOG$_{34–56}$ (P26), another commonly used antigenic peptide (34), and found

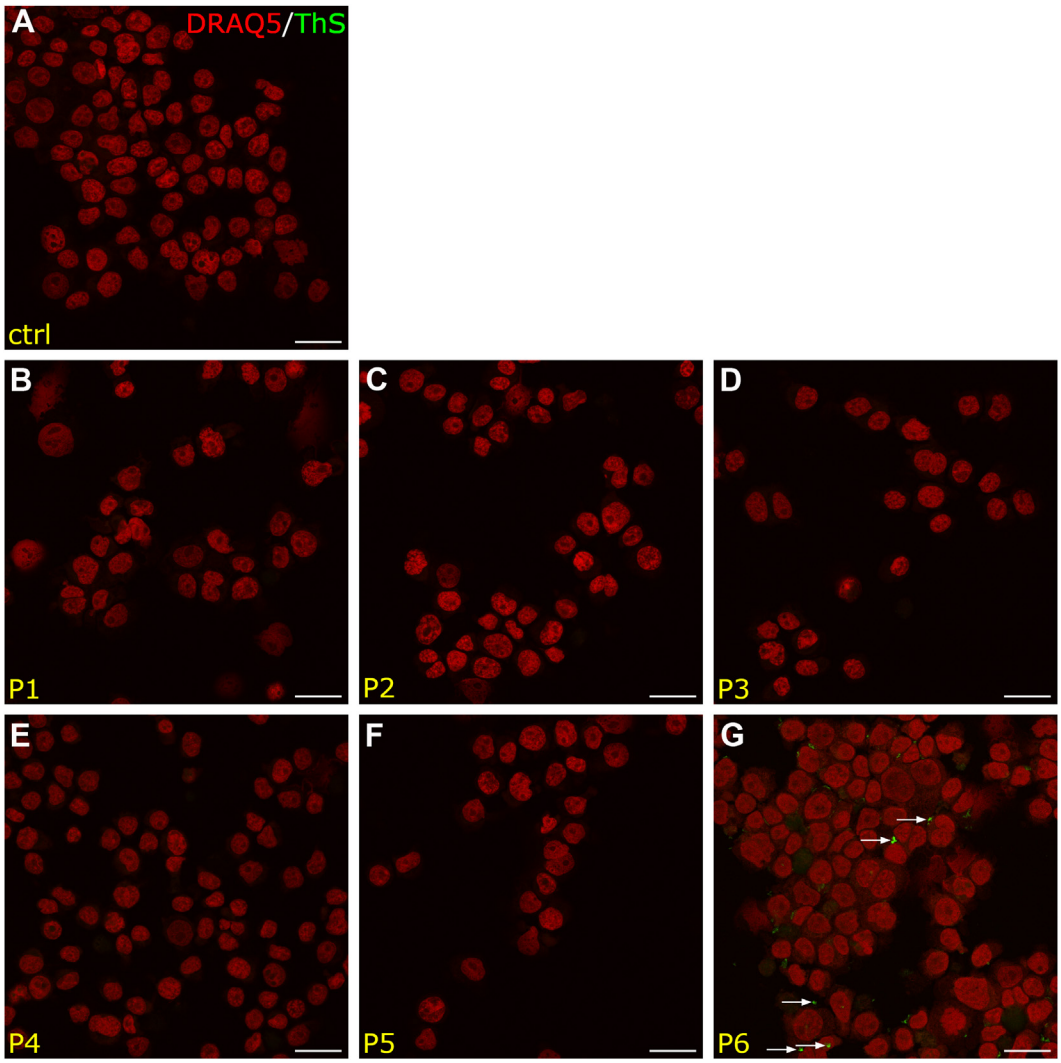

Figure 3. Aggregation of peptides in EBV-infected B cells. EBV-infected B cells cultured at standard conditions were incubated with 50 μm of the indicated peptides for 48 h. Cells were stained with DRAQ5 (*red*) to visualize the nucleus and with thioflavin-S (ThS, *green*) to visualize amyloid-like aggregates. Representative images are shown. Scale bars represent 25 μm. (*A*) control (no peptide), (*B*) $hMOG_{35–55}$ (P1), (*C*) $hMOG_{35–55}$-$Cit_{41,46}$ (P2), (*D*) $hMOG_{35–55}$-$Cit_{46,52}$ (P3), (*E*) $mMOG_{35–55}$ (P4), (*F*) $mMOG_{35–55}$-$Cit_{41,46}$ (P5), and (*G*) $mMOG_{35–55}$-$Cit_{46,52}$ (P6). EBV, Epstein–Barr virus; MOG, myelin oligodendrocyte glycoprotein.

aggregation behavior comparable to $mMOG_{35–55}$-$Cit_{46,52}$ (Fig. S6).

Pro_{42} inhibits cathepsin G degradation of the immunedominant epitope

To enable presentation of the $MOG_{40–48}$ nonapeptide to a T cell, liberation of this epitope from the $MOG_{35–55}$ peptide by proteolysis is essential. On the other hand, destructive antigen processing, meaning proteolytic action within the sequence of $MOG_{40–48}$, will destroy the epitope and prevent T-cell activation.

Cathepsin G (CatG) has been implicated as a crucial protease in the processing of $MOG_{35–55}$. Previous work suggests that this serine protease would destructively process the critical $MOG_{40–48}$ epitope, unless Arg_{46} was citrullinated (22, 24). Destructive processing of myelin autoantigen in B cells has also been implicated as an important mechanism for tolerance to myelin basic protein (35). To more clearly understand the effect of citrullination on the proteolytic degradation of the human and marmoset $MOG_{35–55}$, peptides P1, P3, P4, and P6 were incubated with purified hCatG for 24 h at 37 °C and pH 5.0. At time points 0, 1, 2, 4, and 24 h, a sample was taken and measured by LC–MS. The disappearance of the starting peptides was quantified, and the data were plotted in Figure 6*A*.

Both human peptides P1 and P3 were degraded rather sluggishly. For P1, around 85% of the peptide remained even after 24 h. The citrullinated form of this peptide (P3) is degraded somewhat faster, but more than 50% of the peptide remained after 24 h, indicating that these peptides are stable to hCatG degradation at pH 5.0. In contrast, the marmoset peptide P4 showed considerable faster degradation under the same conditions. While after 4 h 65% of the peptide remained, almost full degradation was achieved after 24 h. The citrullinated peptide P6 was degraded at an even more accelerated

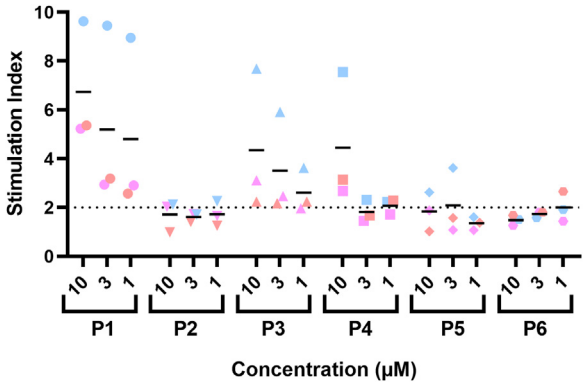

Figure 4. Murine and human citrullinated MOG$_{35-55}$ peptides show distinct T-cell activation in a marmoset B-cell cross-presentation assay. B cells isolated from rhMOG-immunized marmosets were incubated with different peptides at the indicated concentrations for 1 h. Marmoset axillary lymph node (ALN) cells were added, and proliferation was measured using a [^{3}H]thymidine incorporation assay. A stimulation index (ratio of proliferation for stimulated T cells *versus* unstimulated control, SI) was plotted for each condition, and SI >2 was taken as the cutoff for T-cell activation. The experiment was carried out using B cells and ALN cells from three different animals, with individual responses shown as three distinct colors. rhMOG, recombinant human myelin oligodendrocyte glycoprotein .

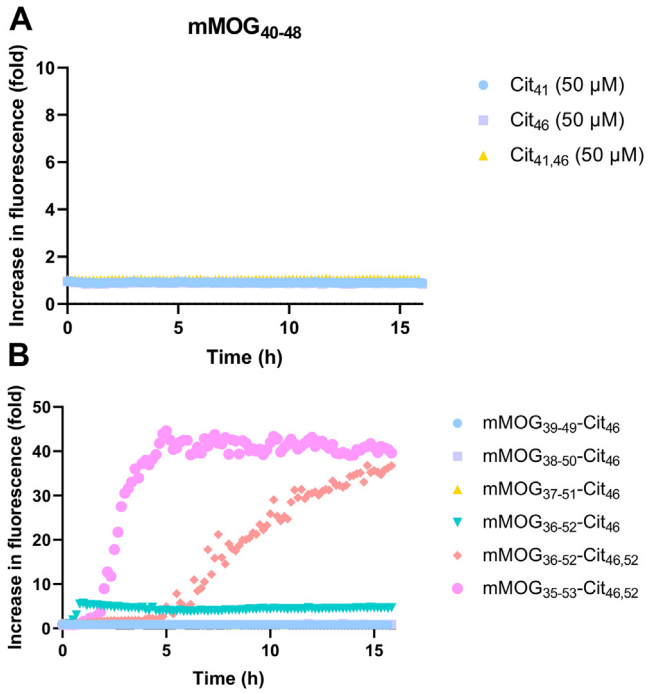

Figure 5. Evaluation of the amyloid-like aggregation of truncated citrullinated mMOG$_{35-55}$ peptides by ThT assay. *A,* ThT aggregation curves of the three citrullinated mMOG$_{40–48}$ epitopes at 50 μM concentration. *B,* ThT aggregation curves of the stepwise extension of the mMOG$_{40–48}$-Cit$_{46}$ epitope. This graph shows representative curves at 50 μM. mMOG, myelin oligodendrocyte glycoprotein from mouse; ThT, thioflavin T.

rate by hCatG, with almost all peptides cleaved after only 4 h incubation.

Using mass spectrometry, the different peptide fragments produced by hCatG were elucidated. The masses of the peptide fragments detected by LC–mass spectrometry were assigned to different parts of the sequences of mMOG$_{35–55}$ or hMOG$_{35–55}$, as shown in Figure 6*B*. Here, major differences in the degradation pattern of these peptides by hCatG were observed. Analysis of the degradation of P4 and P6 indicated that this sequence gets preferentially cleaved between the Phe$_{44}$ and Ser$_{45}$ residues. A second slower cleavage after Tyr$_{40}$ then further degraded the sequence. Both degradation products were absent from the experiments carried out on P1 or P3. Instead, slow cleavage at the C-terminal side, outside the immune-dominant epitope MOG$_{40–48}$, seemed to be preferred here by hCatG.

Discussion

The origins and mechanisms underlaying MS are as of now still poorly understood. To better understand the processes behind neuroinflammation and neurodegeneration, several experimental models have been developed over the years, with MOG-induced EAE being one of the main *in vivo* models used to study MS immunopathogenesis. While these models have not been without criticism (36, 37), they have provided major insights into the cellular and molecular mechanisms underlaying neuroinflammatory and neurodegenerative processes. Since the MOG protein sequences overlap substantially between species, the assumption has often been that the extrapolation of results obtained for the rodent and primate protein could be well translated to the human system. Here, we show that for our earlier obtained results on the amyloid-like aggregation of citrullinated mMOG$_{35–55}$, this translation to the human peptide is not valid.

After finding that the single amino-acid substitution between murine and human MOG$_{35–55}$, a serine-to-proline mutation on position 42, completely abrogated the citrulline-dependent amyloidogenic properties of the peptide, we further investigated the importance of the amino acid at position 42 on this aggregation process. To our surprise, the serine residue on this position appears to be critical for the aggregation, as replacement of serine by structurally closely related amino acids on this position seriously hampered the aggregation (Fig. 2). When staining EBV-infected B cells with ThS, only P6 produced visible aggregates at standard culture conditions. This presents an interesting contrast to our earlier work, where we observed aggregates with derivatives of P4, P5, and P6 upon serum starvation, with P6 also producing larger aggregates than seen here (25). In this previous work, we employed chemical conjugation of the peptide to a fluorophore

Table 2
Overview of synthetic citrullinated shortened and elongated mMOG$_{35–55}$ derivatives

Code	Name	Sequence	Lowest ThT-positive concentration
P17	mMOG$_{40–48}$-Cit$_{41}$	Y*Cit*SPFSRVV	—
P18	mMOG$_{40–48}$-Cit$_{46}$	YRSPFS*Cit*VV	—
P19	mMOG$_{40–48}$-Cit$_{41,46}$	Y*Cit*PPFS*Cit*VV	—
P20	mMOG$_{39–49}$-Cit$_{46}$	WYRPPFS*Cit*VVH	—
P21	mMOG$_{38–50}$-Cit$_{46}$	GWYRPPFS*Cit*VVHL	—
P22	mMOG$_{37–51}$-Cit$_{46}$	VGWYRPPFS*Cit*VVHLY	—
P23	mMOG$_{36–52}$-Cit$_{46}$	EVGWYRPPFS*Cit*VVHLYR	50 μM
P24	mMOG$_{36–52}$-Cit$_{46,52}$	EVGWYRPPFS*Cit*VVHLY*Cit*	25 μM
P25	mMOG$_{35–53}$-Cit$_{46,52}$	MEVGWYRPPFS*Cit*VVHLY*Cit*N	25 μM
P26	mMOG$_{34–56}$-Cit$_{46,52}$	GMEVGWYRSPFS*Cit*VVHLY*Cit* NGKD	3.1 μM

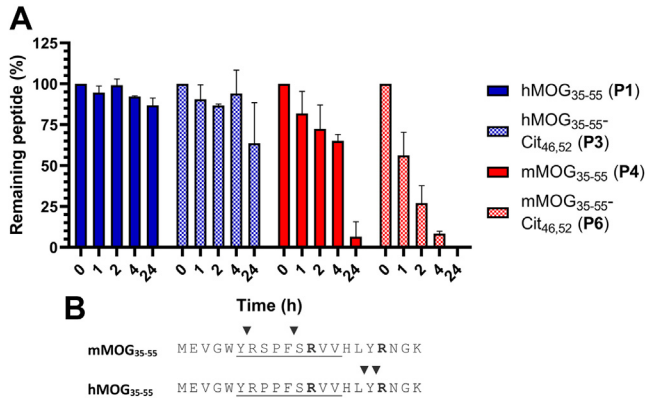

Figure 6. Effect of citrullination on the cathepsin G sensitivity of human and murine MOG$_{35-55}$. *A,* degradation of peptides with human cathepsin G (hCatG) at 37 °C and pH 5.0. Peptides (10 μM) were incubated with hCatG (250 ng/ml), and samples were taken out at the stated time points, and enzymatic activity was stopped by dilution of a 45:45:10 mixture of H_2O/MeCN/TFA. The samples were analyzed using LC–mass spectrometry, and amount of degradation was determined by comparison of peak area against an internal standard. The graph shows the average of two independent experiments for each peptide. *B,* mass spectrometry analysis was used to determine the cleavage sites of hCatG by analyzing the mass spectra of the fragments formed after degradation. *Arrows* indicated detected cleavage sites. The immunodominant epitope MOG$_{40–48}$ is *underlined*, and the citrullinated arginine residues are highlighted in *bold*. MOG, myelin oligodendrocyte glycoprotein.

to localize aggregates; the sensitivity of this approach might be greater than that of the here employed ThS staining. Alternatively, the aggregates seen in our previous article could also bear a mixture of amyloid and nonamyloid aggregates, as thioflavin dyes are selective for the typical cross–beta-sheet secondary structure of amyloids (38). Our microscopy experiments did also further confirm that the peptides derived from human MOG, P1–3, do not form amyloids, as they did not produce ThS-detectable aggregates *in vitro*.

Besides the amyloid-like aggregation of the citrullinated murine peptide, our previous work also described the lack of T-cell response to the different mMOG$_{35–55}$-derived peptides (P4–6) in a crosspresentation assay using EBV-infected B cells as the antigen-presenting cells. Here, we not only repeated this experiment but also included the peptides derived from human MOG (P1–3). We show that while the peptide mMOG$_{35–55}$-Cit$_{46,52}$ (P6) was not capable of inducing T-cell proliferation, as reported previously, the human variant of this peptide (P3) could. Since the marmosets used for this experiment were immunized with wildtype hMOG$_{35–55}$, the origin of this specific response remains to be investigated. Presently, the differences found when comparing the human and murine Cit$_{41,46}$ peptides, that is P3 and P6, were under study. We initially set out to use a docking approach to attempt to understand whether the different MOG$_{40–48}$ epitopes derived from P3 or P6 would bind differently to the Caja-E presentation molecule. While crystal structures of the Caja-E molecule have not been published, the high sequence similarity with the human protein human leukocyte antigen-E meant we could use this protein for the docking model (Fig. S7). However, we were not able to detect any discernable differences in peptide binding that would explain the change in immunological outcome (Fig. S8).

Initially, we surmised that rapid amyloid-like aggregation of peptide P6 could protect the core epitope from being processed in the antigen-presentation pathway, thereby preventing major histocompatibility complex loading and T-cell activation. However, this mechanism would crucially depend on the kinetics of aggregation to be faster than the kinetics of antigen processing. Unexpectedly, analysis of shorter fragments of the aggregating citrullinated mMOG$_{35–55}$ showed that nearly the full-length peptide is required to effectively induce aggregation. This implies that intracellular proteolysis might be capable of preventing the aggregation of free monomeric peptides. Any productive proteolysis of the antigenic peptide that occurs after uptake but before the onset of aggregation could therefore still result in the presentation of a T-cell epitope. As the half-life of a peptide in the cytosol of an antigen-presenting cell has been shown to be in the range of seconds (39), while our data suggest initiation of the aggregation is on the order of minutes *in vitro* (Fig. 1*G*), the kinetics involved do not seem favorable to a scenario where intracellular aggregation prevents peptide processing. This suggests that aggregation takes place before uptake as a more likely scenario, as the rate of uptake of antigen is in the order of minutes as well (40).

As an alternative explanation, we investigated the role of the serine protease CatG, previously implicated to destructively process the core epitope of hMOG$_{40–48}$ unless Arg$_{46}$ was citrullinated (24). Under the conditions we employed, little difference in the degradation between hMOG$_{35–55}$ (P1) and hMOG$_{35–55}$-Cit$_{46}$ (P3) was observed, which were both rather resistant to hCatG degradation; furthermore, the site of degradation was found to be outside the critical hMOG$_{40–48}$ sequence for both peptides. These data suggest that cathepsin G degradation should not interfere with presentation of these peptides. The murine sequence of the peptide (P4) was however rapidly degraded, with citrullination of Arg$_{46}$ and Arg$_{52}$ (P6) further increasing the rate of degradation. For the murine peptides, the site of protease cleavage was found to be within the immunodominant epitope, indicating that the hCatG proteolysis acts as destructive processing for these peptides. The literature on the sequence preference of hCatG showed that an acidic and negatively charged residue is preferred on the P2′ position of the substrate peptide (41), which could explain why neutral citrulline in P2′ results in a higher rate of hydrolysis compared with positively charged arginine. The rapid destruction of the peptide antigen observed for P6 could preclude loading of the epitope into the Caja-E receptor, preventing T-cell activation. Increased stability of antigen to proteolytic mechanisms has been linked to increased ability to stimulate T-cell proliferation (42); our data suggest a strong correlation between the ability to survive hCatG degradation (Fig. 6*A*) and the results of the T-cell proliferation assay (Fig. 4), suggesting such a mechanism is involved here. Indeed, CatG has previously been implicated in the degradation of myelin antigens in B cells, where it was shown that presentation of an immunodominant epitope was prevented by destructive processing of the protein (35). However, the amino acid sequence of human CatG contains different amino acids

at crucial sites when compared with the CatG protein found in other mammals, potentially changing the preferred cleavage sites (43); therefore, the conclusions from this experiment cannot be fully extrapolated to the marmoset system.

In conclusion, we demonstrate, that, after post-translational citrullination, the human and murine sequences of $MOG_{35–55}$ exhibit major differences in biophysical and biochemical behavior, despite the sequence difference being only one amino acid. Our work on synthetic mutants revealed that this amino acid, Ser_{42}, present in the murine but not the human sequence of MOG, is critical for the citrullination-driven aggregation. This same amino acid polymorphism also altered the preference of hCatG-mediated proteolysis. We further showed that shorter fragments of the aggregating murine peptide display severely decreased aggregation propensity. Finally, we showed in an *in vitro* experiment using marmoset material, that a citrullinated peptide derived from the human sequence (P3) induces strong T-cell proliferation, unlike the identically citrullinated murine/marmoset peptide (P6). Our future research will focus on understanding the role of aggregation of $mMOG_{35–55}$ in the development of EAE and furthering our attempts to find the origin of the T-cell proliferation response to $hMOG_{35–55}$-$Cit_{46,52}$ (P3) in the marmoset system. This will help further refine experimental models of autoimmune neuroinflammation like EAE, which in turn will help to better understand the processes underlaying autoimmune central nervous system diseases like MS.

Experimental procedures

General methods for peptide synthesis

Solid-phase peptide synthesis of peptides was carried out using manual synthesis on a 50 μmol on TentaGel S RAM resin (Rapp Polymere GmbH) when a C-terminal carboxamide was desired or on 2′-chloro-trityl chloride polystyrene resin when a C-terminal carboxylic acid was intended. Fmoc-protected amino acids were purchased from either Novabiochem or Sigma–Aldrich. For the amino acids that require side-chain protection, the following protecting groups were used: *t*Bu for Ser, Thr, Tyr, and hydroxyproline; O*t*Bu for Asp and Glu; Trt for Asn, Gln, and His; Boc for Lys and Trp; and Pbf for Arg. To load the first amino acid onto 2′-chloro-trityl chloride resin, 2 equivalents of the desired amino acid together with 5 equivalents of *N*,*N*-diisopropylethylamine dissolved in anhydrous dichloromethane (DCM) (1.25 ml) are added to the resin, which was gently agitated overnight. The loaded resin was then washed with DCM and capped using a mixture of MeOH/*N*,*N*-diisopropylethylamine/DCM (2:1:17) for 1 h. To extend the growing peptide chain, 5 equivalents of Fmoc amino acid was mixed together with an equimolar quantity of 2-(6-chloro-1-H-benzotriazole-1-yl)-1,1,3,3-tetra methylaminium hexaf-luorophosphate in dimethylformamide at a concentration of 0.5 M. Coupling reactions were carried out for 30 to 45 min. Fmoc deprotection was accomplished by repeated treatment with 20% piperidine in dimethylformamide (3 + 7 min). Global deprotection and resin cleavage of peptides were accomplished using a 95:2.5:2.5 mixture of TFA/triisopropylsilane/H_2O for 3 h, followed by precipitation from cold diethyl ether (1:9 ratio TFA to ether) and recovery of the precipitate by centrifugation. Crude tryptophan-containing peptides were dissolved in MilliQ water and lyophilized overnight in order to remove the residual carboxylate. Preparative reverse-phase HPLC on a Waters AutoPurification system (eluent A: H_2O + 0.2% TFA; eluent B: acetonitrile) with a preparative Gemini C18 column (5 μm, 150 × 21.2 mm) yielded the final products. Peptides were characterized using electrospray ionization mass spectrometry on a Thermo Finnigan LCQ Advantage Max LC–mass spectrometry instrument with a Surveyor PDA plus UV detector on an analytical C18 column (Phenomenex, 3 μm, 110 Å, 50 mm × 4.6 mm) in combination with buffers A (H_2O), B (MeCN), and C (1% aqueous TFA). Quality of crude and purified peptides was evaluated with a linear gradient of 10 to 50% B with a constant 10% C over 10 min. Preparative reverse-phase HPLC on a Waters AutoPurification system (eluent A: H_2O + 0.2% TFA; eluent B: acetonitrile) with a preparative Gemini C18 column (5 μm, 150 × 21.2 mm) yielded the final products. All peptides were purified to at least 95% purity as determined by HPLC-UV analysis. An overview of all synthesized peptides, with the yields obtained after RP-HPLC, is given in Table 3.

ThT fluorescence aggregation assays

Aggregation assays were carried out in 96-well plate format using an Infinite M1000 Pro Tecan plate reader. The excitation and emission wavelengths were set to 444 nm and 485 nm, respectively, with a bandwidth of 10 nm. For each peptide under investigation, a 200 μM stock in sodium ascorbate buffer (20 mM, pH = 5) was prepared, and from this stock, a serial diluted one was made using the same buffer. Of these solutions, 199 μl of peptide stock was added into a well and mixed with 1 μl of 1 mM ThT stock solution, prepared in the same NaOAc buffer, for a final dye concentration of 5 μM. Every concentration of peptide was measured in triplicate. The plate was kept at 37 °C, and the fluorescence was measured every 10 min for 16 h. The fluorescence was normalized against a well containing 5 μM ThT in buffer that was measured alongside the assay.

Curve fitting of amyloid-like aggregation

Data obtained from the ThT fluorescence aggregation assay were fitted using GraphPad Prism 8 (GraphPad Software, Inc) according to Equation 1 (31):

$$S(t) = S_0 + \frac{S_\infty - S_0}{1 + e^{-\left[\frac{t - t_{50}}{\tau}\right]}} \quad (1)$$

Where S is the measured ThT fluorescence, t the time, S_0 the fluorescence measured at t = 0, S_∞ the fluorescence measured at the end of the measurement, t_{50} the time at which half maximum fluorescence is reached, and τ a characteristic time constant. t_{lag} was determined by interpolation of the curve for $S(t_{lag}) = 0.1S_\infty$.

Table 3
Overview of all synthesized peptides

No.	Name	Sequence	Scale (μmol)	Yield (μmol)	Yield (%)
P1	$hMOG_{35–55}$	MEVGWYRPPFSRVVHLYRNGK-NH_2	25	6.4	26
P2	$hMOG_{35–55}$-$Cit_{41,46}$	MEVGWY*Cit*PPFS*Cit*VVHLYRNGK-NH_2	25	3.1	12
P3	$hMOG_{35–55}$-$Cit_{46,52}$	MEVGWYRPPFS*Cit*VVHLY*Cit*NGK-NH_2	25	5.6	22
P4	$mMOG_{35–55}$	MEVGWYRSPFSRVVHLYRNGK-NH_2	—[a]	—	—
P5	$mMOG_{35–55}$-$Cit_{41,46}$	MEVGWY*Cit*SPFS*Cit*VVHLYRNGK-NH_2	—[a]	—	—
P6	$mMOG_{35–55}$-$Cit_{46,52}$	MEVGWYRSPFS*Cit*VVHLY*Cit*NGK-NH_2	—[a]	—	—
P7	$MOG_{35–55}$-Ala_{42}-$Cit_{41,46}$	MEVGWY*Cit*APFS*Cit*VVHLYRNGK-NH_2	50	12.1	24
P8	$MOG_{35–55}$-Ala_{42}-$Cit_{46,52}$	MEVGWYRAPFS*Cit*VVHLY*Cit*NGK-NH_2	50	10.6	21
P9	$MOG_{35–55}$-Thr_{42}-$Cit_{41,46}$	MEVGWY*Cit*TPFS*Cit*VVHLYRNGK-NH_2	50	17.5	35
P10	$MOG_{35–55}$-Thr_{42}-$Cit_{46,52}$	MEVGWYRTPFS*Cit*VVHLY*Cit*NGK-NH_2	50	7.9	16
P11	$MOG_{35–55}$-Abu_{42}-$Cit_{41,46}$	MEVGWY*CitAbu*PFS*Cit*VVHLYRNGK-NH_2	50	15.1	30
P12	$MOG_{35–55}$-Abu_{42}-$Cit_{46,52}$	MEVGWYR*Abu*PFS*Cit*VVHLY*Cit*NGK-NH_2	50	19.2	38
P13	$MOG_{35–55}$-Hyp_{42}-$Cit_{41,46}$	MEVGWY*CitHyp*PFS*Cit*VVHLYRNGK-NH_2	50	6.5	13
P14	$MOG_{35–55}$-Hyp_{42}-$Cit_{46,52}$	MEVGWYR*Hyp*PFS*Cit*VVHLY*Cit*NGK-NH_2	50	15.0	30
P15	$hMOG_{35–55}$-Hyp_{43}-$Cit_{41,46}$	MEVGWY*CitPHyp*FS*Cit*VVHLYRNGK-NH_2	50	13.6	27
P16	$hMOG_{35–55}$-Hyp_{43}-$Cit_{46,52}$	MEVGWYRP*Hyp*FS*Cit*VVHLY*Cit*NGK-NH_2	50	11.7	23
P17	$mMOG_{40–48}$-Cit_{41}	Y*Cit*SPFSRVV-OH	50	15.5	31
P18	$mMOG_{40–48}$-Cit_{46}	YRSPFS*Cit*VV-OH	50	14.5	29
P19	$mMOG_{40–48}$-$Cit_{41,46}$	Y*Cit*SPFS*Cit*VV-OH	50	16.4	33
P20	$mMOG_{39–49}$-Cit_{46}	WYRSPFS*Cit*VVH-OH	50	8.6	17
P21	$mMOG_{38–50}$-Cit_{46}	GWYRSPFS*Cit*VVHL-OH	50	13.4	27
P22	$mMOG_{37–51}$-Cit_{46}	VGWYRSPFS*Cit*VVHLY-OH	50	13.7	27
P23	$mMOG_{36–52}$-Cit_{46}	EVGWYRSPFS*Cit*VVHLYR-OH	50	6.7	13
P24	$mMOG_{36–52}$-$Cit_{46,52}$	EVGWYRSPFS*Cit*VVHLY*Cit*-OH	50	13.6	27
P25	$mMOG_{35–53}$-$Cit_{46,52}$	MEVGWYRSPFS*Cit*VVHLY*Cit*N-OH	50	13.7	27
P26	$mMOG_{34–56}$-$Cit_{46,52}$	GMEVGWYRSPFS*Cit*VVHLY*Cit*NGKD-NH_2	50	18.6	37

Synthesis scale and yields are based on manufacturer-provided resin loadings.
[a] Synthesis was previously described in the study by Araman *et al.* (25).

Botulism selective medium cell line culturing

Human EBV-infected lymphoblastoid cell line botulism selective medium (BSM) (ECACC 88052032) was cultured in T75 flasks with RPMI1640 (catalog no.: 21875-034; Gibco) supplemented with 10% heat-inactivated fetal bovine serum (FBS) (Serana; catalog no.: S-FBS-EU-015), 2 mM L-glutamine (catalog no.: 25030-081; Gibco), and 100 U/ml penicillin/streptomycin (catalog no.: 15140-122; Gibco), hereafter called BSM culturing medium. Cultures were maintained at 37 °C and 5% CO_2. Cells were passaged every 2 days by transferring one-third of the cell suspension to a new flask and adding new medium to a total volume of 10 ml. A maximum of 25 ml per flask was used before an experiment was performed.

Seeding and peptide incubation

Cells were collected from the T75 flasks and transferred to a 15 ml tube. Cells were pelleted by centrifugation at 300 rcf for 5 min in an Allegra 21R centrifuge (Beckmann Coulter). The cell pellet was washed once with Dulbecco's PBS (dBS; no calcium, no magnesium; catalog no.: 14190-144; Gibco) and after centrifugation resuspended in BSM culturing medium. About 1.5×10^6 cells per well in a 24-well plate were used for this experiment. Immediately after plating, 50 μM of peptides P1–P6 were added to the cells and diluted in BSM culturing medium. Cells were incubated for 48 h at 37 °C 5% CO_2 before further use.

Cytospin preparation

Cells were transferred to Eppendorf tubes and harvested by centrifuging for 20 min at 1300 rcf at 4 °C. The cell pellet was resuspended in 1 ml dPBS. A cell suspension of 50,000 cells per 100 μl was made in dPBS containing 10% FBS for cytospin preparation. Cytospins were prepared on Shandon Cytoslides (coated; catalog no.: 5991056; ThermoScientific) using the Thermo Shandon Cytospin 3 Centrifuge at 800 rpm for 5 min. Cytospins were dried overnight at room temperature before fixation with 4% paraformaldehyde in PBS for 15 min. Cells were washed three times with PBS before continuing with the ThS staining.

ThS staining

After fixation and washing, cells were incubated with blocking/permeabilization buffer (0.1% bovine serum albumin with 0.5% Triton X-100 in PBS) for 1 h at room temperature. Cells were washed three times with PBS and incubated with freshly made, 0.45 μm filtered, 0.05% ThS (catalog no.: T1892-25G; Sigma) in dPBS for 5 min at room temperature. After removing ThS, cells were washed three times with 70% ethanol and three times with PBS. As a nuclear counterstain, cells were incubated with DRAQ5 (5 μM; catalog no.: 62251; ThermoScientific) in PBS for 15 min at room temperature. Cells were washed once with PBS before mounting a glass coverslip on top with DAKO mounting medium (catalog no.: S302580-02; DAKO Nederland). Slides were imaged using a Leica SP8 confocal laser microscope, lasers 405 nm UV and 638 nm red, at 63× magnification.

T-cell culture assay

Mononuclear cells were isolated from the ALN) from three adult common marmosets (*C. jacchus*). These animals were used in EAE studies, to induce EAE the animals were immunized with MOG34 to 56 (Cambridge Research Biochemicals Ltd) emulsified in IFA. EBV-infected marmoset B cells (BCLs) were used as antigen-presenting cells.

For the proliferation assay, the marmoset BCLs were collected and washed with PBS and irradiated with 70 Gy in RPMI (Gibco) without fetal calf serum. BCLs were plated in 96-well round bottom plates (Greiner) at the concentration of 1.0×10^3 cells/well and incubated for 1 h in an incubator with 5% CO_2 and 37 °C with different concentrations of the peptides (1, 3, and 10 μM), the medium was used as a negative control. After 1 h, thawed mononuclear cells were added to the BCLs at a concentration of 1.0×10^5 cells/well. After 48 h, 25 μl of [methyl-3H] thymidine (0.1 mCi/ml stock; PerkinElmer) was added. About 18 h later, the cells were harvested using a FilterMate Harvester (PerkinElmer) on a microfilter plate. When the plate had dried, 25 μl of Ultima Gold (PerkinElmer) was added and measured on a MicroBeta2 counter (PerkinElmer).

CatG degradation assay

Peptides (10 μM) were dissolved in 200 μl sodium acetate buffer (150 mM, pH 5) and 50 ng of human cathepsin G (Abcam; catalog no.: ab91122) was added as 0.5 μl of a 0.1 mg/ml stock solution in NaOAc buffer (150 mM NaOAc, 150 mM NaCl, pH 5.5). The enzymatic reactions were incubated at 37 °C and gently mixed at 600 RPM using an Eppendorf ThermoMixer C equipped with an Eppendorf SmartBlock for 1.5 ml epps. At specific time points (0, 1, 2, 4, and 24 h), a 20 μl sample was taken. This sample was diluted with a quenching buffer (20 μl, 45:45:10 H_2O/MeCN/TFA) containing 100 μM Cbz-Phe-OH as an internal standard. These samples were analyzed on a Thermo Scientific Vanquish UHPLC coupled to a Thermo Scientific LCQ Fleet ion trap mass spectrometer using a gradient of 5 to 65% B with constant 10% C over 30 min (buffer A: H_2O; buffer B: MeCN; and buffer C: 1% TFA in H_2O). The peak at retention time = 20.4 min was determined to belong to the internal standard, and the ratio of the area under this peak to the area under the starting peptide peak was determined for all time points, using 220 nm as the absorption wavelength. The peak area ratio at $t = 0$ was set to 100%. Newly produced fragments were assigned to peptide sequences by analysis of the electrospray ionization mass spectrum.

Molecular docking

The structures of human leukocyte antigen-E were retrieved from the Protein Data Bank using ICM Molsoft's inbuilt feature. The two entries with a resolution <2.5 Å were visually inspected, and 6GH1 was selected for its slightly better resolution. Of this structure, chain A and peptide P were converted to an ICM object, with "optimize hydrogens" set to true. "Tight" water molecules were retained, leading to a conserved water molecule being present in the binding cleft near the N terminus peptide. This water molecule is present in around half of the structures in the Protein Data Bank. The bound 9-mer epitope was isolated to a separate object and used as template to select the binding cleft by selecting all atoms of the protein in a 5.0 Å radius. A pocket box was defined around this selection using default settings. The $MOG_{40–48}$ epitopes of human (YRPPFSRVV) and mouse (YRSPFSRVV) and their 46-Citr variants were loaded from an SD-file and docked with the "thoroughness" parameter set to 10, the ten best poses were retained. The resulting poses were manually inspected and visualized using the Open Source PyMOL application.

Data availability

All unprocessed experimental data are available upon request from the corresponding authors.

Supporting information—This article contains supporting information.

Author contributions—W. D., W. B., C. A., B. A. 't. H., and S. I. v. K. conceptualization; W. D., A. P. A. J., N. v. D., I. P., C. A., W. B., and S. I. v. K. methodology; W. D., R. C. R., B. A. 't. H., and C. A. formal analysis; N. v. D. and I. P. investigation.

Funding and additional information—W.D. was funded by a Building Blocks of Life grant from the Netherlands Science Foundation (NWO). R. C. R. was funded by an out-of-the box grant of Stichting MS Research. S. I. v. K. was funded by a European Research Council consolidator grant.

Conflict of interest—The authors declare that they have no conflicts of interest with the contents of this article.

Abbreviations—The abbreviations used are: ALN, axillary lymph node; Abu, l-2-aminobutyric acid; BSM, botulism selective medium; CatG, cathepsin G; CFA, complete Freund's adjuvant; DCM, dichloromethane; dPBS, Dulbecco's PBS; EAE, experimental autoimmune encephalomyelitis; EBV, Epstein–Barr virus; FBS, fetal bovine serum; IFA, incomplete Freund's adjuvant; LC-MS, liquid chromatography-mass spectrometry; MOG, myelin oligodendrocyte glycoprotein; MS, multiple sclerosis; ThS, thioflavin S; ThT, thioflavin T.

References

1. Thompson, A. J., Baranzini, S. E., Geurts, J., Hemmer, B., and Ciccarelli, O. (2018) Multiple sclerosis. *Lancet* **391**, 1622–1636
2. Dendrou, C. A., Fugger, L., and Friese, M. A. (2015) Immunopathology of multiple sclerosis. *Nat. Rev. Immunol.* **15**, 545–558
3. Milo, R., and Kahana, E. (2010) Multiple sclerosis: geoepidemiology, genetics and the environment. *Autoimmun. Rev.* **9**, A387–A394
4. Schmidt, H., Williamson, D., and Ashley-Koch, A. (2007) HLA-DR15 haplotype and multiple sclerosis: a HuGE review. *Am. J. Epidemiol.* **165**, 1097–1109
5. Munger, K. L., Levin, L. I., Hollis, B. W., Howard, N. S., and Ascherio, A. (2006) Serum 25-hydroxyvitamin D levels and risk of multiple sclerosis. *J. Am. Med. Assoc.* **296**, 2832–2838
6. Ascherio, A., and Munger, K. L. (2010) Epstein-barr virus infection and multiple sclerosis: a review. *J. Neuroimmune Pharmacol.* **5**, 271–277
7. Bjornevik, K., Cortese, M., Healy, B. C., Kuhle, J., Mina, M. J., Leng, Y., *et al.* (2022) Longitudinal analysis reveals high prevalence of Epstein-Barr virus associated with multiple sclerosis. *Science* **375**, 296–301
8. Lassmann, H., and Van Horssen, J. (2011) The molecular basis of neurodegeneration in multiple sclerosis. *FEBS Lett.* **585**, 3715–3723
9. Bjelobaba, I., Begovic-Kupresanin, V., Pekovic, S., and Lavrnja, I. (2018) Animal models of multiple sclerosis: focus on experimental autoimmune encephalomyelitis. *J. Neurosci. Res.* **96**, 1021–1042

10. Faunce, D. E., Terajewicz, A., and Stein-Streilein, J. (2004) Cutting edge: in vitro-generated tolerogenic APC induce CD8 + T regulatory cells that can suppress ongoing experimental autoimmune encephalomyelitis. *J. Immunol.* **172**, 1991–1995
11. McRae, B. L., Kennedy, M. K., Tan, L.-J., Dal Canto, M. C., Picha, K. S., and Miller, S. D. (1992) Induction of active and adoptive relapsing experimental autoimmune encephalomyelitis (EAE) using an encephalitogenic epitope of proteolipid protein. *J. Neuroimmunol.* **38**, 229–240
12. Peschl, P., Bradl, M., Höftberger, R., Berger, T., and Reindl, M. (2017) Myelin oligodendrocyte glycoprotein: deciphering a target in inflammatory demyelinating diseases. *Front. Immunol.* **8**, 529
13. Jung, J., Dudek, E., and Michalak, M. (2014) The role of N-glycan in folding, trafficking and pathogenicity of myelin oligodendrocyte glycoprotein (MOG). *Biochim. Biophys. Acta* **1853**, 2115–2121
14. Pomeroy, I. M., Matthews, P. M., Frank, J. A., Jordan, E. K., and Esiri, M. M. (2005) Demyelinated neocortical lesions in marmoset autoimmune encephalomyelitis mimic those in multiple sclerosis. *Brain* **128**, 2713–2721
15. Milovanovic, J., Popovic, B., Milovanovic, M., Kvestak, D., Arsenijevic, A., Stojanovic, B., *et al.* (2017) Murine cytomegalovirus infection induces susceptibility to EAE in resistant BALB/c mice. *Front. Immunol.* **8**, 192
16. Jagessar, S. A., Heijmans, N., Blezer, E. L. A., Bauer, J., Weissert, R., and 't Hart, B. A. (2015) Immune profile of an atypical EAE model in marmoset monkeys immunized with recombinant human myelin oligodendrocyte glycoprotein in incomplete Freund's adjuvant. *J. Neuroinflammation.* **12**, 169
17. Vossenaar, E. R., Zendman, A. J. W., Van Venrooij, W. J., and Pruijn, G. J. M. (2003) PAD, a growing family of citrullinating enzymes: genes, features and involvement in disease. *Bioessays* **25**, 1106–1118
18. Moscarello, M. A., Wood, D. D., Ackerley, C., and Boulias, C. (1994) Myelin in multiple sclerosis is developmentally immature. *J. Clin. Invest.* **94**, 146–154
19. Faigle, W., Cruciani, C., Wolski, W., Roschitzki, B., Puthenparampil, M., Tomas-Ojer, P., *et al.* (2019) Brain citrullination patterns and T cell reactivity of cerebrospinal fluid-derived CD4+ T cells in multiple sclerosis. *Front. Immunol.* **10**, 540
20. Luchicchi, A., Hart, B., Frigerio, I., Dam, A., Perna, L., Offerhaus, H. L., *et al.* (2021) Axon-myelin unit blistering as early event in MS normal appearing white matter. *Ann. Neurol.* **89**, 711–725
21. Carrillo-Vico, A., Leech, M. D., and Anderton, S. M. (2010) Contribution of myelin autoantigen citrullination to T cell autoaggression in the central nervous system. *J. Immunol.* **184**, 2839–2846
22. Jagessar, S. A., Holtman, I. R., Hofman, S., Morandi, E., Heijmans, N., Laman, J. D., *et al.* (2016) Lymphocryptovirus infection of nonhuman primate B cells converts destructive into productive processing of the pathogenic CD8 T cell epitope in myelin oligodendrocyte glycoprotein. *J. Immunol.* **197**, 1074–1088
23. Xavier, M., Hauser, S. L., Ludwig, K., Arnold, D. L., Bar-Or, A., Comi, G., *et al.* (2017) Ocrelizumab versus placebo in primary progressive multiple sclerosis. *N. Engl. J. Med.* **376**, 209–220
24. Morandi, E., Jagessar, S. A., 't Hart, B. A., and Gran, B. (2017) EBV infection empowers human B cells for autoimmunity: role of autophagy and relevance to multiple sclerosis. *J. Immunol.* **199**, 435–448
25. Araman, C., van Gent, M. E., Meeuwenoord, N. J., Heijmans, N., Marqvorsen, M. H. S., Doelman, W., *et al.* (2019) Amyloid-like behavior of site-specifically citrullinated myelin oligodendrocyte protein (MOG) peptide fragments inside EBV-infected B-cells influences their cytotoxicity and autoimmunogenicity. *Biochemistry* **58**, 763–775
26. Harrison, R. S., Sharpe, P. C., Singh, Y., and Fairlie, D. P. (2007) Amyloid peptides and proteins in review. In: Amara, S. G., Bamberg, E., Fleischmann, B., Gudermann, T., Hebert, S. C., Jahn, R., *et al.* eds. *Reviews of Physiology, Biochemistry and Pharmacology*, Springer Berlin Heidelberg, Berlin, Heidelberg: 1–77
27. Hatami, A., Monjazeb, S., Milton, S., and Glabe, C. G. (2017) Familial Alzheimer's disease mutations within the amyloid precursor protein alter the aggregation and conformation of the amyloid-β peptide. *J. Biol. Chem.* **292**, 3172–3185
28. Benilova, I., Gallardo, R., Ungureanu, A. A., Cano, V. C., Snellinx, A., Ramakers, M., *et al.* (2014) The Alzheimer disease protective mutation A2T modulates kinetic and thermodynamic properties of amyloid-β (Aβ) aggregation. *J. Biol. Chem.* **289**, 30977–30989
29. Reimann, R. R., Puzio, M., Rosati, A., Emmenegger, M., Schneider, B. L., Valdés, P., *et al.* (2022) Rapid ex vivo reverse genetics identifies the essential determinants of prion protein toxicity. *Brain Pathol.* **3**, e13130
30. Biancalana, M., and Koide, S. (2010) Molecular mechanism of thioflavin-T binding to amyloid fibrils. *Biochim. Biophys. Acta* **1804**, 1405–1412
31. Sabareesan, A. T., and Udgaonkar, J. B. (2014) Amyloid fibril formation by the chain B subunit of monellin occurs by a nucleation-dependent polymerization mechanism. *Biochemistry* **53**, 1206–1217
32. Zurlo, G., Guo, J., Takada, M., Wei, W., and Zhang, Q. (2016) New insights into protein hydroxylation and its important role in human diseases. *Biochim. Biophys. Acta* **1866**, 208–220
33. Westermark, G. T., Johnson, K. H., and Westermark, P. (1999) Staining methods for identification of amyloid in tissue. *Methods Enzymol.* **309**, 3–25
34. Jagessar, S. A., Heijmans, N., Blezer, E. L. A., Bauer, J., Blokhuis, J. H., Wubben, J. A. M., *et al.* (2012) Unravelling the T-cell-mediated autoimmune attack on CNS myelin in a new primate EAE model induced with MOG 34-56 peptide in incomplete adjuvant. *Eur. J. Immunol.* **42**, 217–227
35. Burster, T., Beck, A., Tolosa, E., Marin-Esteban, V., Rötzschke, O., Falk, K., *et al.* (2004) Cathepsin G, and not the asparagine-specific endoprotease, controls the processing of myelin basic protein in lysosomes from human B lymphocytes. *J. Immunol.* **172**, 5495–5503
36. Sriram, S., and Steiner, I. (2005) Experimental allergic encephalomyelitis: a misleading model of multiple sclerosis. *Ann. Neurol.* **58**, 939–945
37. Baker, D., Gerritsen, W., Rundle, J., and Amor, S. (2011) Critical appraisal of animal models of multiple sclerosis. *Mult. Scler.* **17**, 647–657
38. Levine, H. (1995) Thioflavine T interaction with amyloid βsheet structures. *Amyloid* **2**, 1–6
39. Reits, E., Griekspoor, A., Neijssen, J., Groothuis, T., Jalink, K., Van Veelen, P., *et al.* (2003) Peptide diffusion, protection, and degradation in nuclear and cytoplasmic compartments before antigen presentation by MHC class I. *Immunity* **18**, 97–108
40. Kleijmeer, M. J., Ossevoort, M. A., van Veen, C. J., van Hellemond, J. J., Neefjes, J. J., Kast, W. M., *et al.* (1995) MHC class II compartments and the kinetics of antigen presentation in activated mouse spleen dendritic cells. *J. Immunol.* **154**, 5715–5724
41. Thorpe, M., Fu, Z., Chahal, G., Akula, S., Kervinen, J., De Garavilla, L., *et al.* (2018) Extended cleavage specificity of human neutrophil cathepsin G: a low activity protease with dual chymase and tryptase-type specificities. *PLoS One* **13**, e0195077
42. Delamarre, L., Pack, M., Chang, H., Mellman, I., and Trombetta, E. S. (2005) Differential lysosomal proteolysis in antigen-presenting cells determines antigen fate. *Science* **307**, 1630–1634
43. Raymond, W. W., Trivedi, N. N., Makarova, A., Ray, M., Craik, C. S., and Caughey, G. H. (2010) How immune peptidases change specificity: cathepsin G gained tryptic function but lost efficiency during primate evolution. *J. Immunol.* **185**, 5360–5368